Engineering the distinct structure interface of subnano-alumina domains on silica for acidic amorphous silica–alumina toward biorefining

Zichun Wang, Robert Buechel, Yijiao Jiang, Lizhuo Wang, Haimei Xu, Patrice Castignolles, Marianne Gaborieau, Olivier Lafon, Jean-Paul Amoureux, Michael Hunger, et al.

JACS Au
AN OPEN ACCESS JOURNAL OF THE AMERICAN CHEMICAL SOCIETY

pubs.acs.org/jacsau

Article

Engineering the Distinct Structure Interface of Subnano-alumina Domains on Silica for Acidic Amorphous Silica–Alumina toward Biorefining

Zichun Wang, Robert Buechel, Yijiao Jiang, Lizhuo Wang, Haimei Xu, Patrice Castignolles, Marianne Gaborieau, Olivier Lafon, Jean-Paul Amoureux, Michael Hunger, Alfons Baiker,* and Jun Huang*

Cite This: *JACS Au* 2021, 1, 262–271

Read Online

ACCESS | Metrics & More | Article Recommendations | Supporting Information

ABSTRACT: Amorphous silica–aluminas (ASAs) are important solid catalysts and supports for many industrially essential and sustainable processes, such as hydrocarbon transformation and biorefining. However, the wide distribution of acid strength on ASAs often results in undesired side reactions, lowering the product selectivity. Here we developed a strategy for the synthesis of a unique class of ASAs with unvarying strength of Brønsted acid sites (BAS) and Lewis acid sites (LAS) using double-flame-spray pyrolysis. Structural characterization using high-resolution transmission electron microscopy (TEM) and solid-state nuclear magnetic resonance (NMR) spectroscopy showed that the uniform acidity is due to a distinct nanostructure, characterized by a uniform interface of silica–alumina and homogeneously dispersed alumina domains. The BAS population density of as-prepared ASAs is up to 6 times higher than that obtained by classical methods. The BAS/LAS ratio, as well as the population densities of BAS and LAS of these ASAs, could be tuned in a broad range. In cyclohexanol dehydration, the uniform Brønsted acid strength provides a high selectivity to cyclohexene and a nearly linear correlation between acid site densities and cyclohexanol conversion. Moreover, the concerted action of these BAS and LAS leads to an excellent bifunctional Brønsted–Lewis acid catalyst for glucose dehydration, affording a superior 5-hydroxymethylfurfural yield.

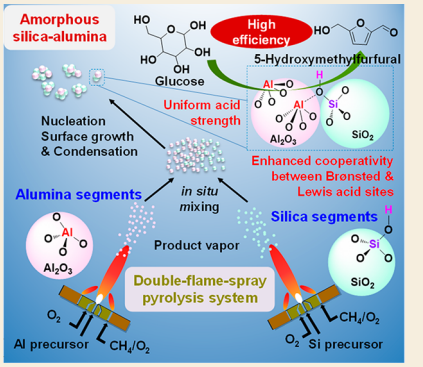

KEYWORDS: *Amorphous silica–alumina, Brønsted and Lewis acidities, double-flame-spray pyrolysis, glucose conversion, cyclohexanol dehydration, solid-state NMR*

1. INTRODUCTION

Silica–alumina catalysts, including amorphous silica–aluminas (ASAs) and zeolites, are the most popular emerging solid acidic catalysts utilized in hydrocarbon transformation and biorefining. In zeolites, the strong Brønsted acid sites (BAS) originate from protons compensating for the negative charges caused by Al^{3+} replacing framework Si^{4+} (Scheme 1a).[1,2] Enhancing the acidity of zeolites by framework dealumination or Al exchange[3−5] introduces Lewis acidic extra-framework Al (EFAl) species, which then act as bifunctional Brønsted–Lewis acidic catalysts. These bifunctional catalysts facilitate the integration of multiple acid-catalyzed reaction steps with high efficiency and promote the conversion of biomass-derived sugars, alcohols, and glycerol into valuable chemicals,[6−8] which have attracted great attention recently. However, the EFAl species generated on zeolite surfaces can easily leach out in liquid-phase reactions, resulting in severe activity loss.[9,10]

Recent advances in the sustainable production of chemicals and fuels from biomass conversion often involve reactions with large molecules. ASAs without diffusional constraints show superior diffusional mass transfer properties for large molecules compared to the microporous zeolites and are thus of great interest in acid-catalyzed conversions of biomass and derivatives.[10−12] In ASAs, the formation of BAS has been widely accepted to originate from an Al atom flexibly coordinated to a neighboring silanol oxygen atom (Scheme 1b)[13−15] or via aluminic pseudobridging silanol (PBS-Al, Scheme 1c, d) at the interface between silica and alumina.[10,16,17] Zeolite-like bridging Si(OH)Al or replacement of an Al atom by Si in Scheme 1c (PBS-Si) are also proposed for BAS formation by theoretical calculation studies but lack direct spectral evidence yet.[18] Moreover, alumina domains on ASAs are associated with the formation of Lewis acid sites (LAS).[19] These properties render ASAs ideal bifunctional Brønsted–Lewis acidic catalysts with versatile acid strengths,

Received: November 18, 2020
Published: February 19, 2021

Scheme 1. Proposed Models for Brønsted Acid Sites (BAS) in Silica–Alumina Catalysts[a]

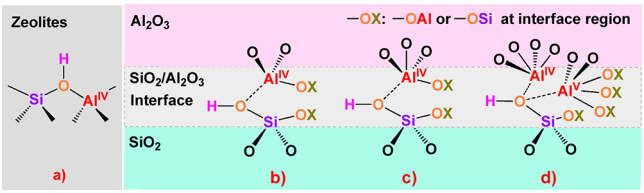

[a](a) BAS consisting of a bridging silanol site bonded to a tetra-coordinated aluminum (Al^{IV}) site (Si(OH)Al) in zeolites.[2] (b) BAS consisting of flexible coordination between silanol oxygen and neighboring Al^{IV}.[20] (c) BAS consisting of a pseudo-bridging silanol (PBS) interacting with an Al^{IV} site.[16] (d) BAS consisting of the synergy of tetra- and penta-coordinated Al (Al^{IV} and Al^{V}) sites with the same SiOH.[10] In b–d, the dotted line does not denote a covalent bond but only the close proximity between O and Al atoms.

high stability, and lower energy barriers compared to zeolites.[10,11]

ASAs are generally prepared by impregnation,[21] sol–gel,[22] precipitation,[23] surface grafting,[14,16,24] and flame-spray pyrolysis (FSP) techniques.[25,26] Using wet-chemistry and post-synthetic modification techniques, the dissolution and recondensation of Al or Si species with surface amorphization result in heterogeneity of Al species inside the silica networks,[16,27] accounting for a wide distribution of acid strengths in ASAs.[16,28,29] Nonuniform acid strengths of solid acids often promote side reactions resulting in lower selectivity and even catalyst deactivation by coking.[14,30,31] Atomic layer deposition (ALD) has been proposed to afford ASAs with uniform BAS strength via the selective reaction of the Si precursor with surface AlOH groups on the alumina support.[14] However, the formation of BAS is strongly hampered by the low density of AlOH groups, which can largely limit the formation of BAS and LAS on ALD-made ASAs. Therefore, the synthesis of ASAs with uniform acid strength and enhanced acidity remains a challenge for both selective and bifunctional Brønsted–Lewis acid catalysis as well as a key in tuning supported metal catalysts with identical electronic properties for high chemoselectivity in hydrogenation reactions.[32]

Uniform acid sites generally require an unvarying local structure of BAS and LAS. Similar domains of alumina on silica or silica on alumina can generate a uniform interface structure for the acid formation. The FSP technique facilitates the preparation of uniform nanoparticles with atomically mixed components or particles with segregated or embedded components in a single step from a liquid precursor solution.[33–35] In contrast to the classical flame spray pyrolysis, where the precursor solution containing all components is sprayed and dispersed into a single flame, double-flame spray pyrolysis (DFSP)[34–40] uses two separate flames and the intersection zone of these flames, where the mixing of the two separately generated aerosols occurs, and can be controlled by proper positioning of the nozzles. This enables the tuning of the intermixing of the components of the synthesized materials on the micro- and/or nanoscale.

Silica–alumina catalysts exhibit high activity in promoting biomass conversions for sustainable production of chemicals and fuel additives.[41–43] For instance, catalytic dehydration of glucose affords 5-hydroxymethylfurfural (HMF), an important building block in the production of liquid alkanes, biofuels, and furan derivatives.[44,45] This production requires glucose isomerization at LAS to fructose, followed by fructose dehydration at BAS to yield HMF,[41,42,46] which is a typical reaction for evaluating the catalytic performance of Brønsted–Lewis acidic catalysts with practical relevance. Dehydration of biomass-derived cyclohexanol to cyclohexene is another example, which is a key precursor to dicarboxylic acids for drug and resin syntheses.[47] The high selectivity to cyclohexene is sensitive to the uniform acid strength of solid acids, which is often utilized as a diagnostic reaction.[14,31]

Herein, we used the DFSP technique to tune the structure of ASAs. We successfully synthesized ASAs made up of uniform alumina domains and a silica–alumina interface, comprising BAS and LAS with virtually unvarying acid strength. The structures of the as-synthesized ASAs were characterized by EDS element mapping and ^{29}Si and ^{27}Al MAS NMR spectroscopy, and their acidities were determined by quantitative ^{1}H and ^{31}P MAS NMR. The catalytic properties of these materials were evaluated using chemical transformations relevant for biomass conversion. A linear relationship between BAS density and cyclohexanol conversion confirms BAS of uniform moderate strength, formed on ASAs, independent of their compositions. The cooperativity of BAS and LAS on DFSP-made ASAs could significantly promote acid-catalyzed glucose dehydration to HMF, providing excellent HMF yields compared to other silica–alumina catalysts.

Table 1. Properties of *d*-SA/*x* Catalysts with Different Si/Al Ratios and Catalytic Results in Cyclohexanol Dehydration

	A^a/m^2/g	SiOH[b]/mmol/g	BAS[b]/mmol/g	LAS[c]/mmol/g	X^d/%	S^d/%	r^d/mol/(m^2 s)
d-SA/5	207	1.2	3×10^{-2}	1.1×10^{-2}	4.4	98.2	3.5×10^{-8}
d-SA/10	218	1.7	7.2×10^{-2}	2.2×10^{-2}	9.5	98.7	7.3×10^{-8}
d-SA/30	221	2.1	12.3×10^{-2}	3.0×10^{-2}	12.9	99.1	9.7×10^{-8}
d-SA/50	218	1.3	9.1×10^{-2}	4.6×10^{-2}	10.4	98.8	8.0×10^{-8}
d-SA/70	207	0.76	8.5×10^{-2}	5.8×10^{-2}	9.2	99.2	7.4×10^{-8}
ALD ASA[e]					9.1		6.6×10^{-8}
CLD ASA[e]							4.7×10^{-8}

[a]*A* is the specific BET surface area. [b]The numbers of total SiOH groups and Brønsted acid sites (BAS) were determined by quantitative ^{1}H MAS NMR measurements. [c]The number of Lewis acid sites (LAS) was quantified from the number of BAS and from the LAS/BAS ratio obtained after simulations of the ^{31}P MAS NMR spectra of TMPO-loaded samples. [d]*X*, *S*, and *r* are the conversion of cyclohexanol, the selectivity to cyclohexene, and the rate of cyclohexanol conversion per unit surface area of ASA and per second, respectively. Conditions: 40 mg of catalyst were added into 2 mL of cyclohexane solution containing 0.1 mmol cyclohexanol; the reaction was carried out at 448 K for 10 min to determine the initial reaction rate *r*. [e]Taken from ref 14.

https://doi.org/10.1021/jacsau.0c00083
JACS Au 2021, 1, 262–271

2. EXPERIMENTAL PROCEDURES

2.1. Catalyst Preparation

Metallorganic precursors, aluminum acetylacetonate ($Al(acac)_3$, ≥99.9%) and tetraethyl orthosilicate (TEOS, ≥99.9%) were purchased from Sigma-Aldrich, and solvents, analytical grade acetic acid and methanol, were from Fluka. All chemicals were used as received. Two precursor solutions were prepared by dissolving the corresponding metal precursors (0.5 M by metal) in a mixture of equal volumes of acetic acid and methanol. The DFSP experimental setup has been described earlier.[36] The geometrical arrangement of the two nozzles and corresponding flames is shown schematically in Figure S1 in the Supporting Information. The nozzles were placed at an angle of 160° to each other and 11 cm apart, such that the aerosol streams were homogeneously mixed at a distance of ca. 34 cm perpendicular to the nozzle. Each precursor solution was pumped through a capillary at a flow rate of 5 mL min^{-1} and was dispersed with 5 L min^{-1} of O_2 into a fine spray. The spray was ignited, with a premixed CH_4/O_2 flame at a volume ratio of 1:2 (total flow rate of the flamelet: 3 L min^{-1}). The nomenclature of the silica–alumina powders is defined as *d*-SA/*x*, where *x* (5, 10, 20, 30, 50, 70) specifies the atom percent of Al in the mixed oxide and *d* indicates that the DFSP system was employed. The reference catalysts Al_2O_3 and H-ZSM-5 were prepared as described in refs 25 and 6, respectively.

2.2. Physical Characterization

Nitrogen adsorption–desorption isotherms. The measurements were performed at 77 K using an Autosorb IQ-C system to determine the specific surface areas. Before measurements, the samples were degassed at 423 K under vacuum to remove adsorbants from the surface. The specific surface areas, determined using the Brunauer–Emmett–Teller (BET) method, are summarized in Table 1.

X-ray Diffraction (XRD). The XRD patterns of *d*-SA/*x* powders were recorded on a Bruker D8 diffractometer with Cu–Kα radiation (λ = 0.154 nm, 35 kV, 40 mA).

Scanning Transmission Electron Microscopy (STEM). The TEM images and STEM-EDS results were acquired on a JEOL-2200FS instrument with 200 kV acceleration tension. The high-angle annular dark-field (HAADF) STEM images were collected on a ThermoFisher Themis Z instrument equipped with a double spherical aberration corrector, and the high tension was 300 kV.

2.3. Solid-State NMR Studies

Before ^{27}Al and ^{29}Si MAS NMR investigations, all samples were exposed overnight at ambient temperature in a desiccator to the saturated vapor of $Ca(NO_3)_2$ solution for definite hydration. Before the ^1H MAS NMR experiments, the samples were filled into glass tubes and dehydrated at 723 K for 12 h at a pressure of less than 10^{-2} bar. These dehydrated samples were then either sealed into the glass tubes or directly loaded with ammonia on a vacuum line. Subsequently, the loaded samples were evacuated at 393 K for 1 h to remove the weakly physisorbed molecules. Then, the samples were transferred into the MAS rotors under dry nitrogen gas inside a glovebox. The MAS rotors were sealed with suitable MAS caps and were then subjected to NMR measurements.

One-dimensional (1D) ^1H, ^{27}Al, and ^{29}Si MAS spectra were recorded at 9.4 T on a Bruker Avance III 400 WB spectrometer at resonance frequencies of 400.1, 104.3, and 79.5 MHz, with sample spinning rates of ν_R = 8, 8, and 4 kHz; rotor diameters of 4, 4, and 7 mm; single-pulse (SP) excitation of 90°, 30°, and 90° flip-angle and recycling delays of RD = 20, 0.5, and 20 s, respectively. High-power ^1H decoupling was applied during ^{29}Si acquisition. Quantitative ^1H MAS NMR measurements were carried out with ν_R = 8 kHz using a zeolite H, Na–Y (35% ion-exchanged) as an external intensity standard. The $^1H-\{^{27}Al\}$ TRAPDOR (transfer of population in double resonance) MAS experiment was performed ν_R = 4 kHz by sending a ^{27}Al irradiation with an rf-field of ν_1 = 50 kHz during the first τ = 200 ms delay of the $\pi/2-\tau-\pi-\tau-$Acq pulse sequence applied to the ^1H nuclei. The data were simulated with the Dmfit software to quantify the different peaks of the 1D spectra.

^{31}P MAS NMR spectra were recorded at 7.05 T on a Bruker DRX 300 spectrometer at 121.5 MHz, with RD = 10 s, 4 mm zirconium oxide rotors, ν_R = 10 kHz, and NS = 6656–16896. Before ^{31}P NMR measurements, samples were dehydrated at 723 K under evacuation conditions overnight. The dehydrated catalysts (ca. 100 mg) were then mixed in a glovebox with TMPO (10 mg) inside the rotor, which was sealed with an O-ring-containing Macor-cap. The sealed sample rotor was finally subjected to thermal treatment at 433 K for 2 h. The data were simulated with the Dmfit software to quantify the different peaks of the 1D spectra.

2D (two-dimensional) ^{27}Al NMR spectra were recorded at 18.8 T on a Bruker Avance III 800 spectrometer equipped with 3.2 mm MAS rotors spinning at ν_R = 20 kHz. The ^{27}Al MQMAS (multiple-quantum MAS) NMR spectra of *d*-SA/10 and *d*-SA/50 were recorded using the three-pulse z-filter pulse sequence.[48] The 2D spectra resulted from the accumulation of respectively NS = 576/192 transients for each of the 8/32 t_1 increments with States-TPPI acquisition, with Δt_1 = 25 μs and RD = 0.5 s. The 2D spectra were sheared with the xfshear program included in the TOPSPIN software. Excitation and reconversion pulses lasted 3 and 1.3 μs, respectively, with ν_1 = 100 kHz, and the central-transition (CT) selective $\pi/2$ last pulse lasted 8 μs with $\nu_1 \approx$ 10 kHz. During ^{27}Al DQ–SQ (double → single-quantum) 2D experiments, CT-selective $\pi/2$ and π-pulses of 8 and 16 μs, that is, an rf amplitude of about 10 kHz, were applied. The ^{27}Al two-spin DQ coherences were excited and reconverted by applying the $BR2_2^1$ pulse sequence,[49] which reintroduces the $^{27}Al-^{27}Al$ dipolar interactions under MAS. The lengths of the excitation and reconversion periods were equal at 800 μs. The rf amplitude applied during the $B2_2^1$ pulse sequence was $\nu_1 \approx$ 3.3 kHz, which corresponds to a nutation frequency of 10 kHz for the ^{27}Al CT. Furthermore, the hyper-secant (HS) scheme was applied before the $BR2_2^1$ excitation,[50] to enhance the ^{27}Al CT polarization by saturating the satellite transitions.[51,52] HS employed a shaped pulse lasting 4 ms with an rf field amplitude of 16 kHz and a frequency sweep of 20 kHz around an offset of 200 kHz with respect to the CT. ^{27}Al DQ–SQ 2D spectra resulted from averaging 14 400 and 3200 transients for *d*-SA/10 and *d*-SA/50 with recycle delay of 2 s, respectively.

2.4. Cyclohexanol Dehydration

Before the reaction, the *d*-SA/*x* catalysts were preheated overnight at 723 K under a nitrogen flow of 50 mL/min. The activated *d*-SA/*x* catalysts (0.04 g) were added into a 2 mL cyclohexane (≥99.5%, Sigma-Aldrich) solution containing 0.1 mmol of cyclohexanol (≥99%, Sigma-Aldrich) in a glass pressure reactor. A 10 mg portion of adamantane was used as an internal standard. The reactor temperature was kept at 448 K by a temperature-controlled oil bath, and the reaction was carried out under stirring for ca. 10 min. The reaction mixtures were then cooled down to room temperature for sample collection. Reaction products were analyzed using a Shimadzu GCMS QP2010 Ultra (Rtx-5MS column 30 m × 0.25 mm × 0.25 μm) and a Shimadzu GC2010 (25QC3/BP1 column 25 m × 0.32 mm × 5 μm).

2.5. HMF from Glucose Dehydration

Glucose (0.06 g, ≥99.5%, Sigma-Aldrich) was dissolved in a mixture of deionized water (0.6 mL) and dimethyl sulfoxide (1.4 mL, DMSO, ≥99.5%, Sigma-Aldrich) as the organic phase. The mixture was then transferred into a glass pressure reactor (25 mL) together with the activated *d*-SA/*x* catalysts (0.02 g). The reaction was performed at 433 K under magnetic stirring for 4 h in a temperature-controlled oil bath. Samples of the reaction mixture were collected after 15, 30, 45, 60, 90, 120, 180, 240 min, diluted with 20.0% (v/v) methanol aqueous solution and filtered for HPLC analysis. The HMF was analyzed by an Agilent 1260 system equipped with a reversed-phase C18 column (Agilent Eclipse Plus Columns, 250 × 4.6 mm, 5 μm) and a multiwavelength detector (DAD) at 284 nm. The mobile phase was 20% (v/v) methanol aqueous solution at a flow rate of 0.6 mL/min. Substrate (glucose) was analyzed using an Agilent 1290 system equipped with a Biorad Aminex HPX-87H column (300 × 7.8 mm, 9

https://doi.org/10.1021/jacsau.0c00083
JACS Au 2021, 1, 262–271

μm) and a refractive index detector (RID). A 0.005 M H_2SO_4 aqueous solution was used as the mobile phase (flow rate: 0.60 mL/min). And, the temperatures of the column and RID were maintained at 333 and 323 K, respectively.

3. RESULTS AND DISCUSSION

3.1. Catalyst Morphology

d-SA catalysts were amorphous as indicated by the XRD patterns (Figure S2). All XRD patterns of *d*-SA/*x* catalysts were dominated by a broad peak due to amorphous silica at $2\theta \approx 25°$,[38] and no crystalline alumina could be detected. Increasing the Al content to 50% and above resulted in a small amount of amorphous alumina, showing diffraction peaks at $2\theta = 46°$ and 67°, which confirm that no crystalline alumina phase was formed, as often detected in ASAs prepared by conventional methods.[23]

Since the formation of small Al domains is invisible by XRD analysis, the ASAs were also examined by EDS element mapping. As expected, Al nanodomains were formed in *d*-SA/10 (Figure 1a and 1b) instead of the homogeneous distribution

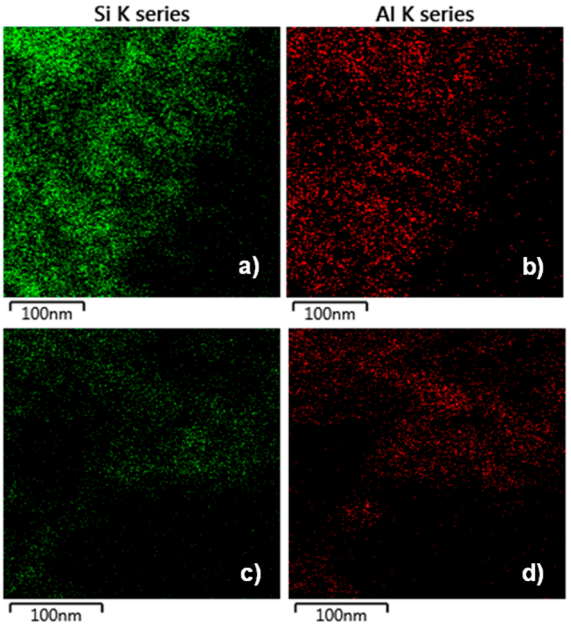

Figure 1. EDS element mapping of (a, b) *d*-SA/10 and (c, d) *d*-SA/50.

of Al and Si atoms in ASAs at low Al/Si ratio.[53] This behavior is further substantiated by more alumina nanodomains formed with increasing Al content, such as in *d*-SA/50 (Figure 1c and 1d), but no obvious alumina phase could be detected at such high Al/Si ratio (Figure S3), in contrast to the significant alumina phase formed in ASAs prepared by wet-chemistry methods by the faster condensation rate of Al−O−Al compared to Al−O−Si.[54]

Since using DFSP could minimize the recondensation between the Si and Al precursors, the resulting surface areas of *d*-SA/*x* catalysts are almost independent of their compositions and are well in the range of the surface areas of pure silica and alumina. Indeed, the BET-surface areas of all *d*-SA/*x* catalysts were in a relatively narrow range of 207−221 m^2/g (Table 1). In contrast, other ASAs often exhibit a wide range of surface areas, strongly dependent on the Al/Si ratios.[26,55]

3.2. Surface Acidity and Local Structure Studies of *d*-SA Catalysts

The local structure of the *d*-SA/*x* catalysts was investigated by ^{29}Si and ^{27}Al 1D MAS NMR spectroscopy. The ^{29}Si spectrum (Figure 2a) of *d*-SA/5 consists of two nonsymmetric peaks

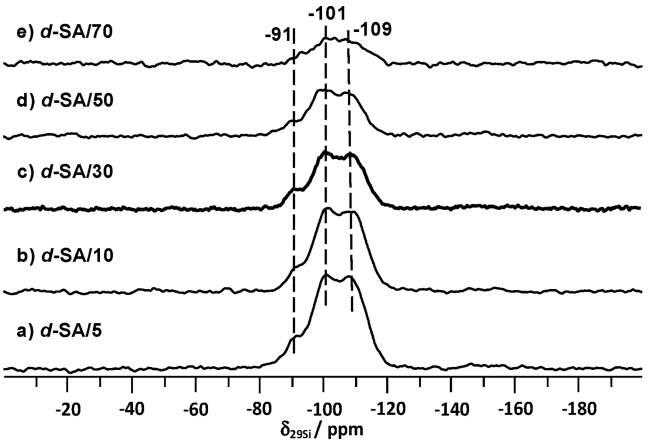

Figure 2. ^{29}Si MAS NMR spectra of *d*-SA/*x* catalysts, with *x* = 5 (a), 10 (b), 30 (c), 50 (d), and 70 (e).

with a broad shoulder, at $\delta_{29Si} = -109$, −101, and −91 ppm, respectively. The line shapes and chemical shifts of these three peaks are nearly independent of the Si/Al ratio, while their intensities decrease from Figure 2a−e due to decreasing Si content. The line shape and chemical shift differences of the ^{29}Si peaks are typical for silica−alumina samples with different Si/Al ratios, including both zeolites and ASAs prepared by various methods.[25,56,57] The systematical shift of the ^{29}Si peaks to higher frequencies with decreasing Si/Al ratio of ASAs is attributed to more Al atoms incorporated into the silica network.[25,26,57,58] Compared to these ASAs, the identical line shapes and chemical shifts of the three ^{29}Si peaks demonstrate that Al domains exert a limiting effect on Si domains in *d*-SA/*x* catalysts. Therefore, the ^{29}Si peaks are mainly controlled by the Si domains, and the peaks at $\delta_{29Si} = -109$, −101, and −91 ppm can be ascribed to Q^4 ($Si(OSi)_4$), Q^3 ($Si(OSi)_3OH$), and Q^2 ($Si(OSi)_2(OH)_2$) species, respectively, similar to those observed with pure silica.[25]

The effect of Si addition on Al domains was investigated by ^{27}Al MAS NMR (Figure 3). All ^{27}Al spectra of *d*-SAs consist of two main resonances at ca. 64 and 7 ppm with a small hump at 35 ppm. These three peaks were analyzed by 3QMAS experiments and assigned to tetrahedral (Al^{IV}), octahedral (Al^{VI}), and pentahedral (Al^{V}) aluminum species, respectively (Figure 4a and b).[48]

^{27}Al 1D and 2D 3QMAS NMR spectra of all *d*-SA/*x* samples are similar and typical for pure Al_2O_3.[25] Moreover, the ^{27}Al−^{27}Al correlations were further investigated in *d*-SA/*x* catalysts by ^{27}Al DQMAS experiments (Figure 4c and d). The 2D spectra are independent of the Si/Al ratio and similar to those reported for Al_2O_3, consisting of mainly Al^{VI}−Al^{VI}, Al^{V}−Al^{VI}, and Al^{IV}−Al^{VI} correlations.[59] In comparison, more complicated correlations between Al species were detected in SA/*x* catalysts due to the strong disturbance of the Al matrix upon silica incorporation.[10] Therefore, we can conclude that the Al distributions and correlations in Al domains were not significantly affected by the Si domains in *d*-SA/*x* catalysts.

https://doi.org/10.1021/jacsau.0c00083
JACS Au 2021, 1, 262−271

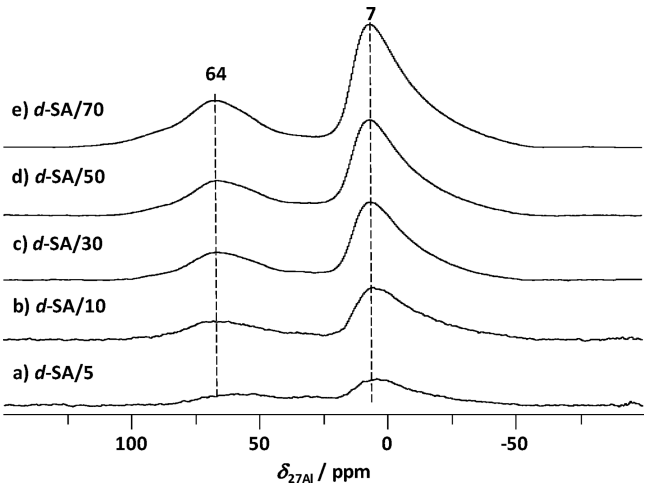

Figure 3. ^{27}Al MAS NMR spectra of *d*-SA/*x* catalysts, with *x* = 5 (a), 10 (b), 30 (c), 50 (d), and 70 (e).

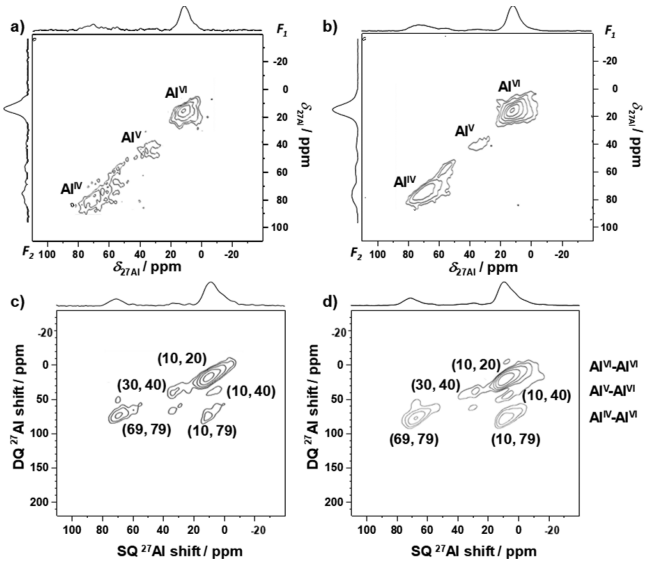

Figure 4. ^{27}Al MQMAS (a, b) and DQMAS (c, d) NMR spectra of *d*-SA/10 (a, c) and *d*-SA/50 (b, d).

Generally, BAS are generated through the spatial proximity between SiOH groups and Al sites in ASAs.[13,14,16] The EDS atom mapping analyses and ^{29}Si and ^{27}Al MAS NMR investigations, suggest a clear separation with an interface between Al and Si domains in *d*-SA/*x* catalysts. Whether there exist spatial proximities between Al sites and SiOH groups on the interface of *d*-SA/*x* catalysts was examined by double-resonance ^{1}H−{^{27}Al} TRAPDOR (transfer of population in double resonance) NMR experiments.[13,60] In these experiments, the applied ^{27}Al irradiation decreases the magnetization of ^{1}H species close to ^{27}Al nuclei, and thus the difference of ^{1}H MAS spectra obtained with and without ^{27}Al irradiation can probe ^{1}H−^{27}Al spin pairs with short distances, such as OH groups interacting with Al species. As shown in Figure 5a, the peak at 1.8 ppm can thus be assigned to SiOH groups having neighboring Al sites.[61]

It has been frequently observed that Al sites can withdraw the electron density from neighboring oxygen atoms of SiOH groups and thereby enhance the acid strength of the SiOH groups, acting as BAS. ^{1}H MAS NMR spectroscopy was often

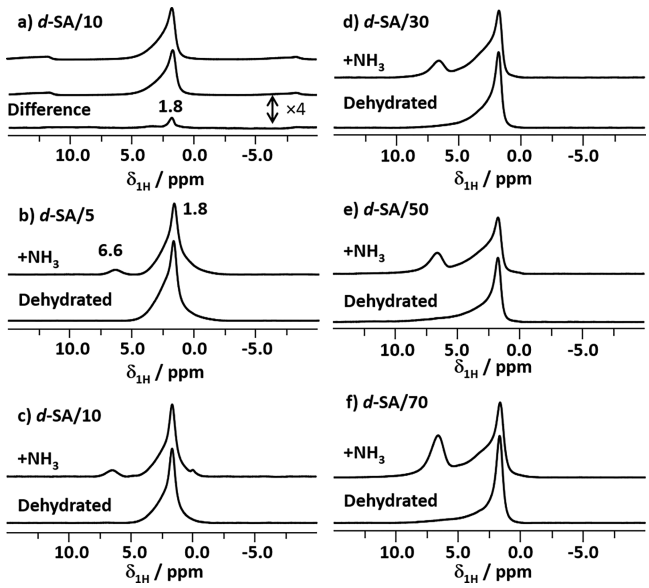

Figure 5. Characterization of surface Brønsted acid sites: ^{1}H MAS NMR spectra of *d*-SA/*x* catalysts. (a) ^{1}H−{^{27}Al} TRAPDOR spectra of dehydrated *d*-SA/10 without (top) and with (middle) ^{27}Al irradiation and their difference spectrum (bottom). (b−f) ^{1}H spectra of dehydrated *d*-SA/*x* recorded before (bottom) and after loading with NH_3 (top); with *x* = 5 (b), 10 (c), 30 (d), 50 (e), and 70 (f). Dehydrated samples were prepared by heating at 723 K for 12 h at a pressure of less than 10^{-2} bar. Loading of dehydrated samples with NH_3 was followed by evacuation and desorption of weakly adsorbed (physisorbed) NH_3 at 393 K for 1 h.

employed to investigate the surface hydroxyl protons.[1,19] As shown in Figures 5b−f, the ^{1}H MAS spectra of dehydrated *d*-SA/*x* catalysts are dominated by a strong SiOH peak at δ_{1H} = 1.8 ppm, which often overlaps with the peak of the acidic SiOH groups (BAS). Adsorption of strong bases, such as NH_3, is a suitable method to probe these surface BAS.[15] Adsorption of ammonia on pure silica is unable to induce any peak change.[62] After Al addition of only 5%, a peak at $\delta_{1H} \approx 6.6$ ppm was immediately observed with *d*-SA/5 (Figure 5b top), assigned to ammonium ions generated by ammonia protonated at BAS. The intensities of the ammonium peaks were utilized to quantify the population densities of BAS listed in Table 1. The densities increased from 3×10^{-2} to 12.3×10^{-2} mmol/g with rising Al content from 5 to 30% and then decreased to 8.5×10^{-2} mmol/g with further increase of the Al content up to 70%. This decrease of BAS density is ascribed to the significant drop of the total number of SiOH groups at low Si loading on the interface. These trends are similar to those reported for ASAs prepared by wet-chemistry methods due to rapid self-condensation of Al nuclei when their content is larger than 30%,[63] forming an alumina phase.[64,65] However, no such alumina phase could be observed with *d*-SA/*x* catalysts. Instead, more Al nanodomains were generated with increasing Al loading in *d*-SA/*x* catalysts (Figures 1 and 3), which is proposed to promote the formation of LAS.

^{31}P MAS NMR using TMPO as a probe molecule is a suitable spectroscopic method to distinguish different types of acid sites with various strength.[5,66,67] Often, the chemical shift of TMPO increases with a higher acid strength of BAS. As shown in Figures 6a and b, a strong peak at 45 ppm and a broad hump at ca. 68 ppm were observed on *d*-SA/5 and *d*-SA/10. The first peak is assigned to physisorbed TMPO,[68]

https://doi.org/10.1021/jacsau.0c00083
JACS Au 2021, 1, 262−271

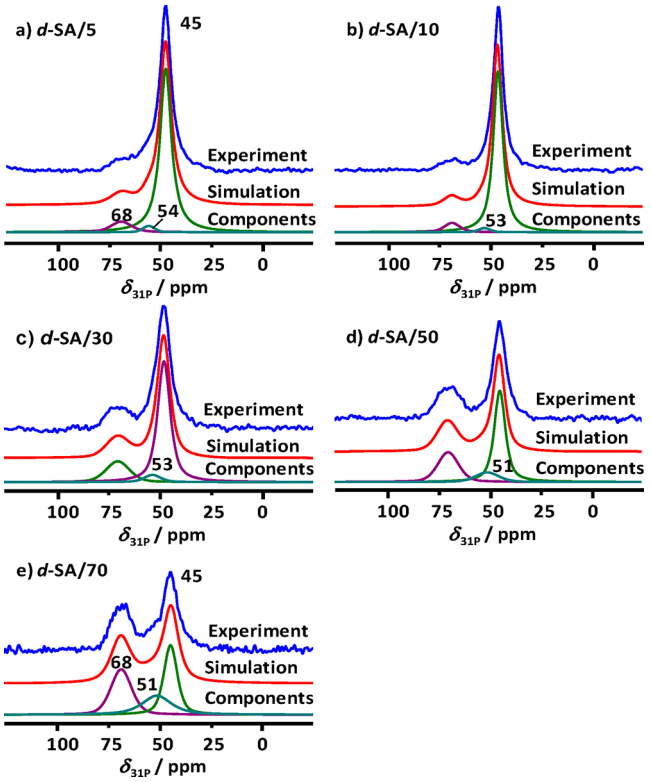

Figure 6. ^{31}P MAS NMR spectra of dehydrated (773 K) *d*-SA/*x* loaded with TMPO: with *x* = 5 (a), 10 (b), 30 (c), 50 (d), and 70 (e).

while that at ca. 68 ppm is attributed to TMPO adsorbed at weak BAS.[66,69] Moreover, a broad hump at ca. $\delta_{31P} \approx 51$ ppm was detected, which is typical for TMPO strongly adsorbed at LAS.[66] Similarly, the strongly adsorbed ammonia at LAS on ASAs could result in a broad hump at $\delta_{1H} \approx 3$ ppm,[31] which is also observed in Figure S4. The increase of the broad peak at higher Al content enables one to assign it as TMPO adsorbed at LAS.

The simulation results shown in Figure 6 are based on these observations. The identical acid strength of BAS on all *d*-SA/*x* catalysts is thereby probed with the same chemical shift of 68 ppm. The acid strength of LAS on *d*-SA/*x* catalysts is slightly higher than that on flame-made (50 ppm) and commercial alumina (48 ppm).[66] This is attributed to the fact that LAS are present in nanodomains, compared to their existence in nanoparticles, and the large alumina phase of the two other samples, respectively. Moreover, the density of LAS can be determined by that of BAS and by the LAS/BAS ratio obtained in ^{1}H and ^{31}P MAS experiments, since only one TMPO molecule can be adsorbed per BAS or LAS. The quantitative results, summarized in Table 1, show that the number of LAS (LAS density) correlates well with the Al content.

3.3. Formation of Acid Sites on *d*-SA Catalysts

Figure 7 shows a simplified scheme of the possible particle formation pathways occurring in the ASA syntheses using DFSP. As shown, the liquid Si and Al precursors are fed through the independent nozzles, which spray the liquid precursors into the two flames. The precursors are vaporized and intermixed in the zone where the flames overlap. Primary small nanoclusters are formed by nucleation, surface growth, and/or condensation. BAS formation is proposed to occur in the mixing zone by surface interaction between Al sites in

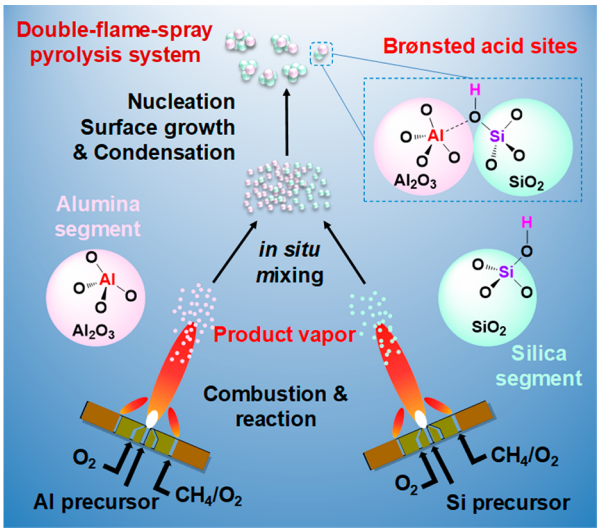

Figure 7. Schematic of possible particle formation pathways during the aerosol synthesis by injecting Si and Al precursors from two independent nozzles (DFSP setup) for nanoparticle synthesis. The dotted line for BAS does not denote a covalent bond but only the close proximities between O and Al atoms.

proximity to SiOH groups on the interface. These domains grow by coagulation−agglomeration, forming finally aggregates and agglomerates in the final mixed oxide powders (Figure S2).

Decoupling of the interaction between Al and Si precursors during DFSP synthesis was demonstrated by the characteristics of silica and alumina domains that are independent of the compositions of *d*-SA/*x* catalysts, as shown in Figures 1−4. Previous DFSP studies show that the metal species (e.g., Pd) are selectively located in the vicinity of SiOH groups on the surface,[38] due to the high electron density of the hydroxyl oxygen. Similarly, we propose that the LAS prefer to interact with surface SiOH groups on the interface, which is confirmed by ^{1}H−{^{27}Al} TRAPDOR experiments (Figure 5a). Since the local structure of interfaces in *d*-SA/*x* catalysts is similar and does not depend on their compositions (Si/Al ratio), the acid strengths of BAS and LAS are uniform for all prepared ASAs.

Employing the DFSP technique with the given conditions, the number of uniform alumina domains as well as the interfacial area in silica−aluminas increased with higher Al content. Consequently, the population density of BAS and LAS on ASAs could be improved by using DFSP. For example, the BAS density on *d*-SA/*x* catalysts is up to 6 times higher than those obtained by other methods.[14,70] The LAS/BAS ratio of *d*-SA/*x* catalysts could be flexibly tuned, and both the density of LAS and BAS could be boosted, which contrasts the behavior of ALD-made ASAs, where the LAS density decreases monotonously with increasing BAS density. The number of uniform BAS on ASAs prepared by ALD is also limited by the small amount of AlOH groups on low-surface area alumina (large alumina support, particle size < 3 μm).

3.4. Cyclohexanol Dehydration to Cyclohexene

d-SA/*x* catalysts with uniform and moderate BAS and LAS strengths have been successfully prepared in this work. Dehydration of biomass-derived cyclohexanol with high selectivity to cyclohexene (Scheme 2) is a typical test reaction to characterize BAS with uniform and moderate strength, since

https://doi.org/10.1021/jacsau.0c00083
JACS Au 2021, 1, 262−271

Scheme 2. Catalytic Dehydration of Cyclohexanol to Cyclohexene

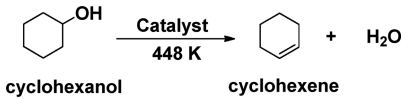

the product distribution is sensitive to strong BAS, resulting in side reactions and catalyst deactivation.[14,71]

The catalytic activity of *d*-SA/*x* catalysts was evaluated using cyclohexanol dehydration, and the results are summarized in Table 1. As previously reported,[14,31] Al_2O_3 is virtually inactive under the conditions applied here. GC analysis mainly detected cyclohexene, without carbonaceous deposits, which are typically formed with strong solid acids.[72] With *d*-SA/*x* catalysts, the selectivity to cyclohexene (98−99%) is much higher than that achieved with corresponding catalysts prepared by single-nozzle FSP and coprecipitation methods (38−95%), which both show a wide distribution of BAS strength.[31] The high cyclohexene selectivity achieved with DFSP is in line with the unvarying and moderate BAS strength, which is independent of the compositions of *d*-SA/*x* catalysts.

Increasing the BAS density on *d*-SA/*x* catalysts could promote their activity in cyclohexanol dehydration. Figure S5 shows that the conversion and reaction rate, *r*, of cyclohexanol almost linearly increases with the density of BAS. As an example, the reaction rate *r* on *d*-SA/30 (9.7×10^{-8} mol/(m^2 cat. s)) is 6 and 3 times higher than corresponding rates observed on pure alumina (1.6×10^{-8} mol/(m^2 cat. s))[31] and *d*-SA/5 (3×10^{-8} mol/(m^2 cat. s)), respectively. Further increase of the Al content up to 70% resulted in a decrease of *r* to 7.4×10^{-8} mol/(m^2 cat. s) due to the decline of the BAS density. At a similar selectivity to cyclohexene, *d*-SA/*x* catalysts showed up to 1.5 times higher *r* than those reported for SiO_x/Al_2O_3 prepared by ALD and CLD techniques.[14]

3.5. HMF Production from Glucose Dehydration

The bifunctional Brønsted−Lewis acidic properties of *d*-SA/*x* catalysts were examined using the glucose dehydration to HMF (Scheme 3 and Table 2). Employing *d*-SA/*x* catalysts

Scheme 3. Proposed Reaction Pathway for Catalytic Dehydration of Glucose to HMF[a]

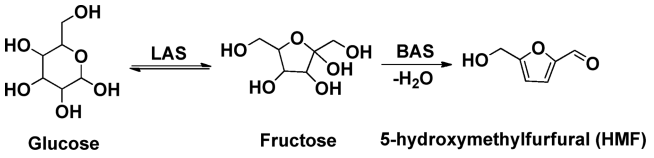

[a]LAS: Lewis acid sites. BAS: Brønsted acid sites.

could more efficiently promote the glucose conversion compared to other ASAs with similar Al content,[10] for instance, 50 vs 23% and 91 vs 70%, at 10 and 50% Al content, respectively, after 2 h of reaction under similar conditions. The higher glucose conversion is attributed to the higher density of LAS generated by the DFSP synthesis,[12,25] which is further demonstrated in Figure S6 by a nearly linear correlation between glucose conversion and the density of LAS.

It emerges from the reaction data in Table 2 that the HMF selectivity determined after 2 h of reaction increases gradually up to that of the *d*-SA/70 catalyst. This increase of the HMF selectivity with BAS density (Table 1) became more

Table 2. Catalytic Performance of ASAs in the Conversion of Glucose to HMF[a]

	conversion[b]/%	yield[b]/%	selectivity[b]/%
d-SA/5	34 (90)	9 (36)	26.5 (40)
d-SA/10	50 (92)	14 (43)	28.1 (45)
d-SA/30	78 (100)	30 (64)	38.5 (64)
d-SA/50	91 (100)	38 (54)	41.8 (54)
d-SA/70	100 (100)	45 (49)	45.9 (49)
ASA/30[c]	64	25	39

[a]Conditions under stirring at 433 K: 20 mg of catalyst were added to a mixture of deionized water (0.6 mL) and DMSO (1.4 mL) containing 60 mg of glucose. [b]The conversion of glucose, selectivity, and yield to HMF are provided after 2 h of reaction, and the results after 4 h of reaction are given in parentheses. [c]ASA/30 with an Al/Si ratio of 30/70 was obtained from ref 25.

prominent after 4 h of reaction, and maximum selectivity was already observed for *d*-SA/30 (Table 2, Figure S7). HMF is generated by dehydration of fructose, which depends on the preceding step, the glucose isomerization to fructose. On *d*-SA/*x* catalysts, the LAS density increases at higher Al content, while the maximum BAS density is obtained at 30% Al loading. This could explain the observed HMF selectivity behavior since BAS and LAS have a different influences on the reaction steps 1 (glucose isomerization) and 2 (fructose isomerization).

The dependence of the HMF selectivity at full conversion of glucose on the LAS/BAS ratio in the range 0.24−0.68, shown in Figure 8, indicates that at a low LAS/BAS ratio the HMF

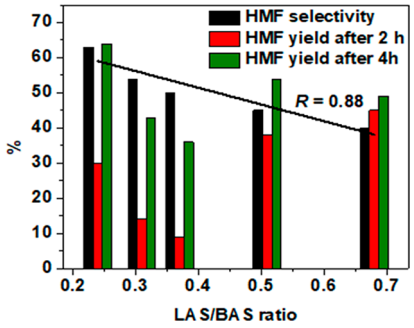

Figure 8. Selectivity at full conversion of glucose and yield of HMF vs the ratio of LAS/BAS (*R* = coefficient of determination). Conditions under stirring at 433 K: 20 mg of the catalyst were added into a mixture of deionized water (0.6 mL) and DMSO (1.4 mL) containing 60 mg of glucose.

formation is enhanced. This result is similar to that obtained using mesoporous silica−alumina catalysts, but with a much lower LAS/BAS ratio (0.1−0.47).[73] However, the increase of the LAS/BAS ratio from 0.53 to 1.7 in H-Beta zeolites improves the HMF selectivity from 36 to 55% at 453 K, after 4 h in H_2O−DMSO (9:1)/THF (1:3),[74] while an increase of the LAS/BAS ratio from 0.25 to 2.5, in ion-exchanged (Fe(II) and Cu(II)) H-ZSM-5, enhances the HMF selectivity from 13 to 35% at 468 K for 150 min of reaction in a water/methyl isobutyl ketone biphasic system.[75] This has been attributed to a higher LAS/BAS ratio which could inhibit the formation of humins or oligomers at strong BAS.[76] This hypothesis has been confirmed by comparing the HMF selectivities obtained using *d*-SA/70 with only moderate BAS, and ASA/70 with strong BAS but a much lower LAS/BAS ratio. Indeed, both catalysts afforded similar HMF selectivities, 47% and 50%, respectively,

https://doi.org/10.1021/jacsau.0c00083
JACS Au 2021, 1, 262−271

at ca. 85% glucose conversion. This further substantiates that *d*-SA/*x* catalysts with unvarying moderate BAS and lower LAS/BAS ratios are selective for generating HMF in glucose conversion. As shown in Figure 8, the HMF yields seem to be rather independent of the LAS/BAS ratio. The rareness of LAS on *d*-SA/5 and *d*-SA/10 hampers the isomerization of glucose to fructose, forcing the HMF yields to remain less than 14% after 2 h, but then rapidly increase to 36−43% after 4 h of reaction. *d*-SA/50 and *d*-SA/70 with a 1.5−3 times higher amount of LAS than *d*-SA/5 and *d*-SA/10 enabled the HMF yield to increase from 38 to 45% after 2 h of reaction. Compared to ASA/*x* catalysts, *d*-SA/*x* catalysts provide a higher LAS density and, thus, promote the formation of HMF, as shown in Table 2.

d-SA/30 with the highest density of BAS, unvarying moderate strength, and a nearly optimized LAS/BAS ratio afforded the highest HMF yield (63%) after 4 h of reaction among the *d*-SA/*x* catalysts. This yield is much higher than that achieved with other silica−alumina based catalysts reported so far,[74,75,77] indicating that *d*-SA/*x* catalysts are promising bifunctional catalysts for glucose dehydration. Particularly, compared to ASAs prepared by sol−gel and coprecipitation techniques, up to 1.5 times higher HMF yield is achieved under the same conditions after 2 h of reaction.[10] This property has been attributed to the concerted action of BAS and LAS on *d*-SA/*x* catalysts. As shown in Figure 9, LAS

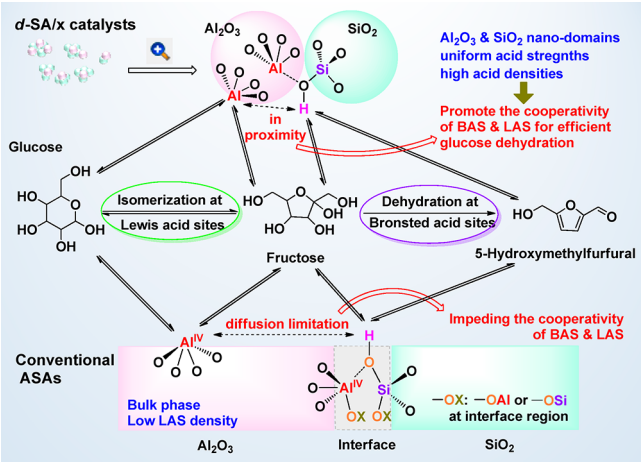

Figure 9. Proposed reaction mechanism for glucose dehydration into HMF over ASA and *d*-SA/*x* catalysts.

and BAS commonly originate from different phases in ASAs. This impedes the surface diffusion of the fructose formed at LAS on the alumina phase to the BAS existing at the interface between alumina and silica phases for subsequent dehydration yielding HMF. Note that concentrated reactant/intermediates at the strong BAS or LAS would likely result in the formation of humins or oligomers.[73,76] On *d*-SA/*x* catalysts, the BAS with uniform moderate strength are generated by the interaction of very small domains of alumina and silica constituents, which is expected to promote the fructose formed at LAS and its diffusion to neighboring BAS for dehydration to HMF. The cooperative action of BAS and LAS also provides an almost twice higher HMF selectivity and yield with *d*-SA/30 than with ASA/30 (Al/Si = 30/70) at full conversion of glucose. This is remarkable since ASA/30 possesses mainly moderately strong BAS and a similar population density (ASA 11.1 × 10^{-2} mmol/g, compared to *d*-SA/30 12.3 × 10^{-2} mmol/g). The reusability of *d*-SA/30 was tested under identical conditions, and after five recycles, no significant activity loss was detected (Figure S8). This demonstrates that the interaction of the nanodomains of alumina and silica constituents can generate in *d*-SA/30 a uniform BAS and LAS proximity, thereby promoting the efficiency of the transformation of glucose to HMF.

4. CONCLUSION

In this work we reported a route to synthesize a new class of high-performance ASAs, containing BAS and LAS with uniform strength, using double-flame spray pyrolysis (DFSP). The structural characterization of as-synthesized *d*-SA catalysts by EDX element mapping and various solid-state NMR techniques revealed that BAS of similar strength are generated on an interface formed by Al sites on nanodomains of alumina interacting with neighboring SiOH groups on small silica domains. Moreover, the small silica and alumina nanodomains generated in the aerosol during flame synthesis give rise to a high surface area as well as a large silica−alumina interface, and alumina nanodomains promoting both the formation of BAS and LAS. The obtained BAS population density is up to 6 times higher than that of ASAs prepared by conventional methods, and the LAS density increases with increasing Al content.

The existence of BAS with uniform moderate strength formed on *d*-SA catalysts has been substantiated by the high selectivity to cyclohexene achieved in the dehydration of cyclohexanol. In the bifunctional Brønsted−Lewis acid-catalyzed glucose conversion, an HMF yield of 63% was achieved on *d*-SA/30 with a nearly optimal LAS/BAS ratio. This is the highest HMF yield among silica−aluminas (including ASAs with strong BAS) reported under similar conditions. This novel route for synthesizing silica−alumina catalysts with uniform BAS and LAS strengths facilitates an adaptive tuning of the density of BAS and LAS, which is crucial for efficient conversion of hydrocarbons and biomass. DFSP proved to be a powerful method for tailoring the structure of mixed oxides at the submicron- and/or nanoscale, as shown in this work on the tuning of the acidic properties of ASAs.

■ ASSOCIATED CONTENT

Supporting Information

The Supporting Information is available free of charge at https://pubs.acs.org/doi/10.1021/jacsau.0c00083.

Additional catalysts preparation methods, XRD patterns, HAADF images of SA/10, catalytic reaction results, and recycling studies (PDF)

■ AUTHOR INFORMATION

Corresponding Authors

Alfons Baiker − *Institute for Chemical and Bioengineering, Department of Chemistry and Applied Bioscience, ETH Zürich, Hönggerberg, HCI, Zurich CH-8093, Switzerland;* orcid.org/0000-0003-1408-464X; Email: alfons.baiker@chem.ethz.ch

Jun Huang − *Laboratory for Catalysis Engineering, School of Chemical and Biomolecular Engineering & Sydney Nano Institute, The University of Sydney, Sydney, NSW 2006, Australia;* orcid.org/0000-0001-8704-605X; Email: jun.huang@sydney.edu.au

https://doi.org/10.1021/jacsau.0c00083
JACS Au 2021, 1, 262−271

Authors

Zichun Wang − *Laboratory for Catalysis Engineering, School of Chemical and Biomolecular Engineering & Sydney Nano Institute, The University of Sydney, Sydney, NSW 2006, Australia; Department of Engineering, Macquarie University, Sydney, New South Wales 2109, Australia;* orcid.org/0000-0002-4280-2787

Robert Buechel − *Particle Technology Laboratory, Department of Mechanical and Process Engineering, ETH Zuürich, CH-8092 Zuürich, Switzerland;* orcid.org/0000-0003-2627-4352

Yijiao Jiang − *Department of Engineering, Macquarie University, Sydney, New South Wales 2109, Australia;* orcid.org/0000-0002-6191-9825

Lizhuo Wang − *Laboratory for Catalysis Engineering, School of Chemical and Biomolecular Engineering & Sydney Nano Institute, The University of Sydney, Sydney, NSW 2006, Australia*

Haimei Xu − *Department of Engineering, Macquarie University, Sydney, New South Wales 2109, Australia*

Patrice Castignolles − *Australian Centre for Research on Separation Science (ACROSS), School of Science, Western Sydney University, Parramatta, New South Wales 2150, Australia*

Marianne Gaborieau − *Australian Centre for Research on Separation Science (ACROSS), School of Science, Western Sydney University, Parramatta, New South Wales 2150, Australia;* orcid.org/0000-0002-9991-8123

Olivier Lafon − *Univ. Lille, CNRS, UMR 8181, UCCS-Unité de Catalyse et de Chimie du Solide, F-59000 Lille, France; Institut Universitaire de France, 75231 Paris, France;* orcid.org/0000-0002-5214-4060

Jean-Paul Amoureux − *Univ. Lille, CNRS, UMR 8181, UCCS-Unité de Catalyse et de Chimie du Solide, F-59000 Lille, France; Bruker Biospin, 67166 Wissembourg, France; Riken NMR Science and Development Division, Yokohama 230-0045, Kanagawa, Japan*

Michael Hunger − *Institute of Chemical Technology, University of Stuttgart, D-70550 Stuttgart, Germany;* orcid.org/0000-0002-1870-2743

Complete contact information is available at: https://pubs.acs.org/10.1021/jacsau.0c00083

Author Contributions

J.H. and Y.J. designed the study. R.B. prepared the samples. Z.W., P.C., M.G., O.L., M.H., and J.H. performed the NMR experiments and structural assignments. Z.W. and H.X. performed the catalytic experiments and data analysis. L.W. performed the microscopy study. J.H. and A.B. supervised the scientific work. J.H. and Z.W. wrote the draft, and O.L., J.P.A., and A.B. revised the paper.

Notes

The authors declare no competing financial interest.

ACKNOWLEDGMENTS

J.H. and Z.W. acknowledge the financial support from Australian Research Council Discovery Projects (DP150103842, DP180104010, and DE190101618). J.H. thanks the University of Sydney SOAR fellowship, Sydney Nano Grand Challenge, and the International Project Development Funding.

REFERENCES

(1) Jiang, Y.; Huang, J.; Dai, W.; Hunger, M. *Solid State Nucl. Magn. Reson.* **2011**, *39*, 116−141.
(2) Xu, J.; Wang, Q.; Li, S.; Deng, F. Solid-State NMR Characterization of Acid Properties of Zeolites and Solid Acid Catalysts. In *Solid-State NMR in Zeolite Catalysis*; Springer: Singapore, 2019; pp 159−197.
(3) Huang, J.; Jiang, Y.; Marthala, V. R. R.; Thomas, B.; Romanova, E.; Hunger, M. *J. Phys. Chem. C* **2008**, *112*, 3811−3818.
(4) Yu, Z.; Li, S.; Wang, Q.; Zheng, A.; Jun, X.; Chen, L.; Deng, F. *J. Phys. Chem. C* **2011**, *115*, 22320−22327.
(5) Wang, Z.; O'Dell, L. A.; Zeng, X.; Liu, C.; Zhao, S.; Zhang, W.; Gaborieau, M.; Jiang, Y.; Huang, J. *Angew. Chem., Int. Ed.* **2019**, *58*, 18061−18068.
(6) Wang, Z.; Wang, L.; Jiang, Y.; Hunger, M.; Huang, J. *ACS Catal.* **2014**, *4*, 1144−1147.
(7) Wang, C.; Chu, Y.; Xu, J.; Wang, Q.; Qi, G.; Gao, P.; Zhou, X.; Deng, F. *Angew. Chem., Int. Ed.* **2018**, *57*, 10197−10201.
(8) Kim, K. D.; Wang, Z.; Jiang, Y.; Hunger, M.; Huang, J. *Green Chem.* **2019**, *21*, 3383−3393.
(9) Dapsens, P. Y.; Mondelli, C.; Perez-Ramirez, J. *ChemSusChem* **2013**, *6*, 831−839.
(10) Wang, Z.; Li, T.; Jiang, Y.; Lafon, O.; Liu, Z.; Trébosc, J.; Baiker, A.; Amoureux, J.-P.; Huang, J. *Nat. Commun.* **2020**, *11*, 225.
(11) Larmier, K.; Chizallet, C.; Maury, S.; Cadran, N.; Abboud, J.; Lamic-Humblot, A. F.; Marceau, E.; Lauron-Pernot, H. *Angew. Chem., Int. Ed.* **2017**, *56*, 230−234.
(12) Wang, Z.; Jiang, Y.; Baiker, A.; Huang, J. *ACS Catal.* **2013**, *3*, 1573−1577.
(13) Luo, Q.; Deng, F.; Yuan, Z. Y.; Yang, J.; Zhang, M. J.; Yue, Y.; Ye, C. H. *J. Phys. Chem. B* **2003**, *107*, 2435−2442.
(14) Mouat, A. R.; George, C.; Kobayashi, T.; Pruski, M.; van Duyne, R. P.; Marks, T. J.; Stair, P. C. *Angew. Chem., Int. Ed.* **2015**, *54*, 13346−13351.
(15) Wang, Z.; Ling, H.; Shi, J.; Stampfl, C.; Yu, A.; Hunger, M.; Huang, J. *J. Catal.* **2018**, *358*, 71−79.
(16) Chizallet, C.; Raybaud, P. *Angew. Chem., Int. Ed.* **2009**, *48*, 2891−2893.
(17) Perras, F. A.; Wang, Z.; Kobayashi, T.; Baiker, A.; Huang, J.; Pruski, M. *Phys. Chem. Chem. Phys.* **2019**, *21*, 19529−19537.
(18) Chizallet, C. *ACS Catal.* **2020**, *10*, 5579−5601.
(19) Wang, Z. C.; Jiang, Y. J.; Lafon, O.; Trebosc, J.; Kim, K. D.; Stampfl, C.; Baiker, A.; Amoureux, J. P.; Huang, J. *Nat. Commun.* **2016**, *7*, 13820.
(20) Omegna, A.; van Bokhoven, J. A.; Prins, R. *J. Phys. Chem. B* **2003**, *107*, 8854−8860.
(21) Locus, R.; Verboekend, D.; d'Halluin, M.; Dusselier, M.; Liao, Y. H.; Nuttens, N.; Jaumann, T.; Oswald, S.; Mafra, L.; Giebeler, L.; Sels, B. *ChemCatChem* **2018**, *10*, 1385−1397.
(22) Williams, M. F.; Fonfe, B.; Sievers, C.; Abraham, A.; van Bokhoven, J. A.; Jentys, A.; van Veen, J. A. R.; Lercher, J. A. *J. Catal.* **2007**, *251*, 485−496.
(23) Keller, T. C.; Arras, J.; Haus, M. O.; Hauert, R.; Kenvin, A.; Kenvin, J.; Pérez-Ramírez, J. *J. Catal.* **2016**, *344*, 757−767.
(24) Caillot, M.; Chaumonnot, A.; Digne, M.; Poleunis, C.; Debecker, D. P.; van Bokhoven, J. A. *Microporous Mesoporous Mater.* **2014**, *185*, 179−189.
(25) Huang, J.; van Vegten, N.; Jiang, Y.; Hunger, M.; Baiker, A. *Angew. Chem., Int. Ed.* **2010**, *49*, 7776−7781.
(26) Wang, Z.; Jiang, Y.; Jin, F.; Stampfl, C.; Hunger, M.; Baiker, A.; Huang, J. *J. Catal.* **2019**, *372*, 1−7.
(27) Kitrell, J. R. *Hydrotreating catalyst comprising an ultra-stable crystalline zeolitic molecular sieve component,and methods for making and using said catalyst*. United States Patent 3536605, 1968.
(28) Crepeau, G.; Montouillout, V.; Vimont, A.; Mariey, L.; Cseri, T.; Mauge, F. *J. Phys. Chem. B* **2006**, *110*, 15172−15185.
(29) Caillot, M.; Chaumonnot, A.; Digne, M.; van Bokhoven, J. A. *J. Catal.* **2014**, *316*, 47−56.

(30) Trombetta, M.; Busca, G.; Rossini, S.; Piccoli, V.; Cornaro, U.; Guercio, A.; Catani, R.; Willey, R. J. *J. Catal.* **1998**, *179*, 581−596.
(31) Wang, Z.; Jiang, Y.; Stampfl, C.; Baiker, A.; Hunger, M.; Huang, J. *ChemCatChem* **2020**, *12*, 287−293.
(32) Wang, Z.; Kim, K.-D.; Zhou, C.; Chen, M.; Maeda, N.; Liu, Z.; Shi, J.; Baiker, A.; Hunger, M.; Huang, J. *Catal. Sci. Technol.* **2015**, *5*, 2788−2797.
(33) Mädler, L.; Kammler, H. K.; Mueller, R.; Pratsinis, S. E. *J. Aerosol Sci.* **2002**, *33*, 369−389.
(34) Liu, S.; Mohammadi, M. M.; Swihart, M. T. *Chem. Eng. J.* **2021**, *405*, 126958.
(35) Koirala, R.; Pratsinis, S. E.; Baiker, A. *Chem. Soc. Rev.* **2016**, *45*, 3053−3068.
(36) Buchel, R.; Strobel, R.; Krumeich, F.; Baiker, A.; Pratsinis, S. E. *J. Catal.* **2009**, *261*, 201−207.
(37) Strobel, R.; Piacentini, M.; Mädler, L.; Maciejewski, M.; Baiker, A.; Pratsinis, S. E. *Chem. Mater.* **2006**, *18*, 2532−2537.
(38) Wang, Z.; Pokhrel, S.; Chen, M.; Hunger, M.; Mädler, L.; Huang, J. *J. Catal.* **2013**, *302*, 10−19.
(39) Kim, K. D.; Pokhrel, S.; Wang, Z. C.; Ling, H. J.; Zhou, C. F.; Liu, Z. W.; Hunger, M.; Mädler, L.; Huang, J. *ACS Catal.* **2016**, *6*, 2372−2381.
(40) Horlyck, J.; Pokhrel, S.; Lovell, E.; Bedford, N. M.; Mädler, L.; Amal, R.; Scott, J. *Catal. Sci. Technol.* **2019**, *9*, 4970−4980.
(41) Swift, T. D.; Nguyen, H.; Erdman, Z.; Kruger, J. S.; Nikolakis, V.; Vlachos, D. G. *J. Catal.* **2016**, *333*, 149−161.
(42) Wang, Z.; Huang, J. Brønsted-Lewis Acids for Efficient Conversion of Renewables. In *Production of Biofuels and Chemicals with Bifunctional Catalysts*; Fang, Z., Smith, R.L., Li, H., Eds.; Springer Nature: Singapore, 2017; pp 99−136.
(43) Roman-Leshkov, Y.; Moliner, M.; Labinger, J. A.; Davis, M. E. *Angew. Chem., Int. Ed.* **2010**, *49*, 8954−8957.
(44) Corma, A.; Iborra, S.; Velty, A. *Chem. Rev.* **2007**, *107*, 2411−2502.
(45) Mika, L. T.; Csefalvay, E.; Nemeth, A. *Chem. Rev.* **2018**, *118*, 505−613.
(46) Otomo, R.; Tatsumi, T.; Yokoi, T. *Catal. Sci. Technol.* **2015**, *5*, 4001−4007.
(47) Lesage, G.; Peñate, I. Q.; Franceschi, S.; Perez, E.; Garrigues, J.-C.; Poux, M.; Cognet, P. *Catal. Today* **2020**, *346*, 40−45.
(48) Amoureux, J. P.; Fernandez, C.; Steuernagel, S. Z filtering in MQMAS NMR. *J. Magn. Reson., Ser. A* **1996**, *123*, 116−118.
(49) Wang, Q.; Hu, B.; Lafon, O.; Trébosc, J.; Deng, F.; Amoureux, J. P. *J. Magn. Reson.* **2009**, *200*, 251−260.
(50) Siegel, R.; Nakashima, T. T.; Wasylishen, R. E. *Chem. Phys. Lett.* **2004**, *388*, 441−445.
(51) Madhu, P. K.; Goldbourt, A.; Frydman, L.; Vega, S. *Chem. Phys. Lett.* **1999**, *307*, 41−47.
(52) Yao, Z.; Kwak, H.-T.; Sakellariou, D.; Emsley, L.; Grandinetti, P. J. *Chem. Phys. Lett.* **2000**, *327*, 85−90.
(53) Wang, Z.; Jiang, Y.; Yi, X.; Zhou, C.; Rawal, A.; Hook, J.; Liu, Z.; Deng, F.; Zheng, A.; Hunger, M.; Baiker, A.; Huang, J. *Sci. Bull.* **2019**, *64*, 516−523.
(54) Kriesel, J. W.; Sander, M. S.; Tilley, T. D. *Adv. Mater.* **2001**, *13*, 331−335.
(55) Xu, B.; Sievers, C.; Lercher, J. A.; van Veen, J. A. R.; Giltay, P.; Prins, R.; van Bokhoven, J. A. *J. Phys. Chem. C* **2007**, *111*, 12075−12079.
(56) Wang, Z.; Wang, L.; Zhou, Z.; Zhang, Y. Y.; Li, H. T.; Stampfl, C.; Liang, C. H.; Huang, J. *J. Phys. Chem. C* **2017**, *121*, 15248−15255.
(57) Valla, M.; Rossini, A. J.; Caillot, M.; Chizallet, C.; Raybaud, P.; Digne, M.; Chaumonnot, A.; Lesage, A.; Emsley, L.; van Bokhoven, J. A.; Coperet, C. *J. Am. Chem. Soc.* **2015**, *137*, 10710−10719.
(58) Huang, J.; Jiang, Y.; van Vegten, N.; Hunger, M.; Baiker, A. *J. Catal.* **2011**, *281*, 352−360.
(59) Lee, D.; Takahashi, H.; Thankamony, A. S. L.; Dacquin, J.-P.; Bardet, M.; Lafon, O.; De Paepe, G. *J. Am. Chem. Soc.* **2012**, *134*, 18491−18494.
(60) Grey, C. P.; Vega, A. J. *J. Am. Chem. Soc.* **1995**, *117*, 8232−8242.
(61) Xu, M.; Wang, W.; Seiler, M.; Buchholz, A.; Hunger, M. *J. Phys. Chem. B* **2002**, *106*, 3202−3208.
(62) Wang, Z.; Jiang, Y.; Rachwalik, R.; Liu, Z.; Shi, J.; Hunger, M.; Huang, J. *ChemCatChem* **2013**, *5*, 3889−3896.
(63) Hunger, M.; Freude, D.; Pfeifer, H.; Bremer, H.; Jank, M.; Wendlandt, K. P. *Chem. Phys. Lett.* **1983**, *100*, 29−33.
(64) Matsumoto, A.; Chen, H.; Tsutsumi, K.; Grun, M.; Unger, K. *Microporous Mesoporous Mater.* **1999**, *32*, 55−62.
(65) Eimer, G. A.; Pierella, L. B.; Monti, G. A.; Anunziata, O. A. *Catal. Lett.* **2002**, *78*, 65−75.
(66) Lang, S.; Benz, M.; Obenaus, U.; Himmelmann, R.; Hunger, M. *ChemCatChem* **2016**, *8*, 2031−2036.
(67) Zheng, A.; Liu, S. B.; Deng, F. *Chem. Rev.* **2017**, *117*, 12475−12531.
(68) Hayashi, S.; Kojima, N. *Microporous Mesoporous Mater.* **2011**, *141*, 49−55.
(69) Huang, S. J.; Yang, C. Y.; Zheng, A. M.; Feng, N. D.; Yu, N. Y.; Wu, P. H.; Chang, Y. C.; Lin, Y. C.; Deng, F.; Liu, S. B. *Chem. - Asian J.* **2011**, *6*, 137−148.
(70) Hensen, E. J. M.; Poduval, D. G.; Degirmenci, V.; Ligthart, D.; Chen, W. B.; Mauge, F.; Rigutto, M. S.; van Veen, J. A. R. *J. Phys. Chem. C* **2012**, *116*, 21416−21429.
(71) He, J.; Zhao, C.; Lercher, J. A. *J. Catal.* **2014**, *309*, 362−375.
(72) Garcia-Ochoa, F.; Santos, A. *Ind. Eng. Chem. Res.* **1993**, *32*, 2626−2632.
(73) Li, X. C.; Xia, Q. N.; Nguyen, V. C.; Peng, K. H.; Liu, X. H.; Essayem, N.; Wang, Y. Q. *Catal. Sci. Technol.* **2016**, *6* (20), 7586−7596.
(74) Otomo, R.; Yokoi, T.; Kondo, J. N.; Tatsumi, T. *Appl. Catal., A* **2014**, *470*, 318−326.
(75) Moreno-Recio, M.; Santamaria-Gonzalez, J.; Maireles-Torres, P. *Chem. Eng. J.* **2016**, *303*, 22−30.
(76) Ordomsky, V. V.; Sushkevich, V. L.; Schouten, J. C.; van der Schaaf, J.; Nijhuis, T. A. *J. Catal.* **2013**, *300*, 37−46.
(77) Wang, J.; Ren, J.; Liu, X.; Xi, J.; Xia, Q.; Zu, Y.; Lu, G.; Wang, Y. *Green Chem.* **2012**, *14*, 2506−2512.

NOTE ADDED AFTER ISSUE PUBLICATION

This article was initially published with an incorrect copyright statement and was corrected on or around May 5, 2021.

https://doi.org/10.1021/jacsau.0c00083
JACS Au 2021, 1, 262−271

Supporting Information

Engineering the Distinct Structure Interface of Subnano-alumina Domains on Silica for Acidic Amorphous Silica–Alumina toward Biorefining

Zichun Wang,[1,2] Robert Buechel,[3] Yijiao Jiang,[2] Lizhuo Wang,[1] Haimei Xu,[2] Patrice Castignolles,[4] Marion Gaborieau,[4] Olivier Lafon,[5,6] Jean-Paul Amoureux,[5,7,8] Michael Hunger,[9] Alfons Baiker,[10*] and Jun Huang[1*]

[1] Laboratory for Catalysis Engineering, School of Chemical and Biomolecular Engineering & Sydney Nano Institute, The University of Sydney, Sydney, NSW 2006, Australia

[2] Department of Engineering, Macquarie University, Sydney, New South Wales 2109, Australia

[3] Particle Technology Laboratory, Department of Mechanical and Process Engineering, ETH Zürich, Sonneggstrasse 3, CH-8092 Zürich, Switzerland.

[4] School of Science and Health, Western Sydney University, Sydney, New South Wales 2751, Australia

[5] Univ. Lille, CNRS, UMR 8181, UCCS-Unité de Catalyse et de Chimie du Solide, F-59000 Lille, France

[6] Institut Universitaire de France, 1, rue Descartes, 75231 Paris Cedex 05, France

[7] Bruker Biospin, 34, rue de l'industrie, 67166 Wissembourg, France

[8] Riken NMR Science and Development Division, Yokohama, 230-0045 Kanagawa, Japan.

[9] Institute of Chemical Technology, University of Stuttgart, D-70550 Stuttgart, Germany

[10] Institute for Chemical and Bioengineering, Department of Chemistry and Applied Bioscience, ETH Zürich, Hönggerberg, HCI, CH-8093, Switzerland

Preparation of H-ZSM-5 zeolite

All chemicals used for ZSM-5 synthesis, such as NaOH (> 99.99 %), tetrapropylammonium hydroxide (TPAOH, 1.0 M in H_2O), silicic acid (> 99.9 %), sodium aluminate (50~56 % Al_2O_3, 37~45 % Na_2O), ammonium hydroxide solution (28 % NH_3 in H_2O) and $Al(NO_3)_3$ (≥ 98 %) were obtained from Sigma-Aldrich. Aluminum-containing Na-ZSM-5 was synthesized via a hydrothermal route.[1] First, seeding gel was prepared by thoroughly mixing deionized water, NaOH, TPAOH, and silicic acid solution in the molar ratio of 116:1.6:1:5, respectively. The resulting mixture was stirred for 1 h under ambient temperature, followed by aging at 100 °C for 16 h. A mixture consisting of water, sodium hydroxide, sodium aluminate, silicic acid, and seeding gel with the respective molar ratio of 375:1.7:0.3:9.4:1 was stirred at ambient temperature for 1 h. Then the resulting gel was placed into an autoclave and aged at 180 ^oC for 40 h. The products were recovered by filtration, washing, and drying at 105 ^oC for 24 h. Finally, to completely remove organic compounds, the as-synthesized samples were calcined in a flow of synthetic air (58 L/h, 20 vol% oxygen) at 550 ^oC with a heating rate of 1 ^oC/min for 5 h. Then, ammonia exchange with the obtained solid product was employed to prepare H–form zeolites, as described in our earlier work.[2] Briefly, the solid product was mixed with a specified amount of 0.1 M NH_4NO_3 aqueous solution and stirred at 80 °C for 3 h. After filtration and washing with deionized water, until no nitrate ions could be detected anymore, the obtained product was dried at room temperature overnight. The above procedure was repeated four times to ensure an ion-exchange degree > 99 % in the final product.

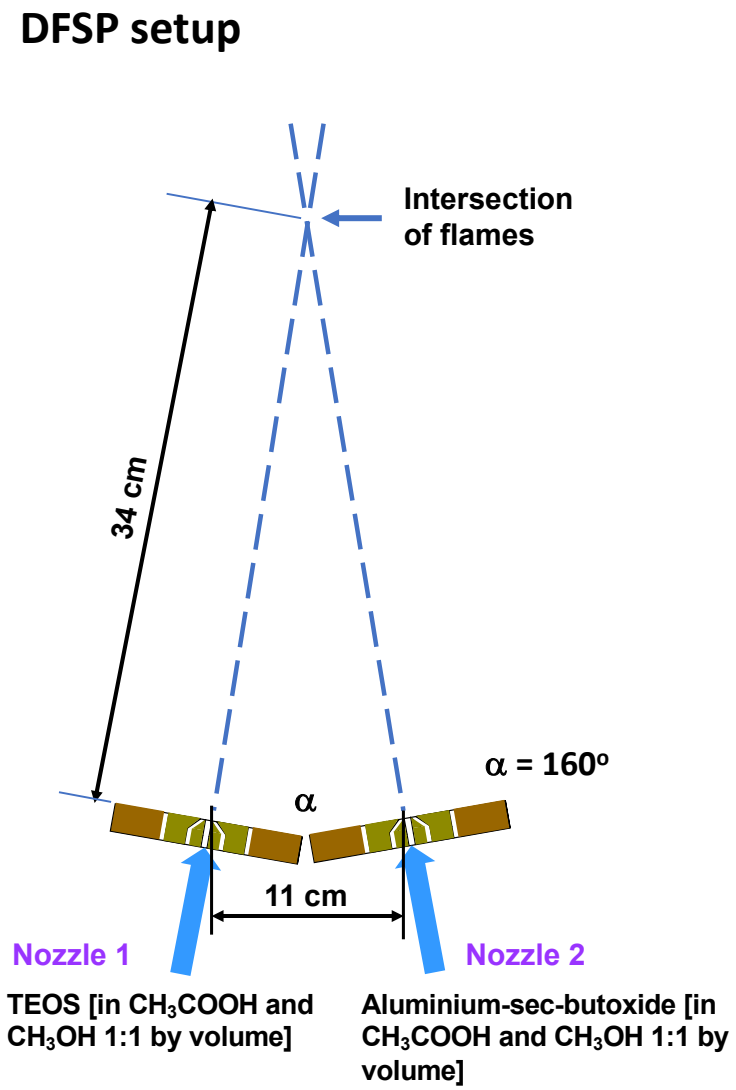

Fig. S1. Geometrical arrangement of nozzles in DFSP setup used for the synthesis of *d*-SA/x catalysts. A photo of the setup used is shown in Ref. 3 (Fig. 11).

XRD analysis of d-SA/x catalysts

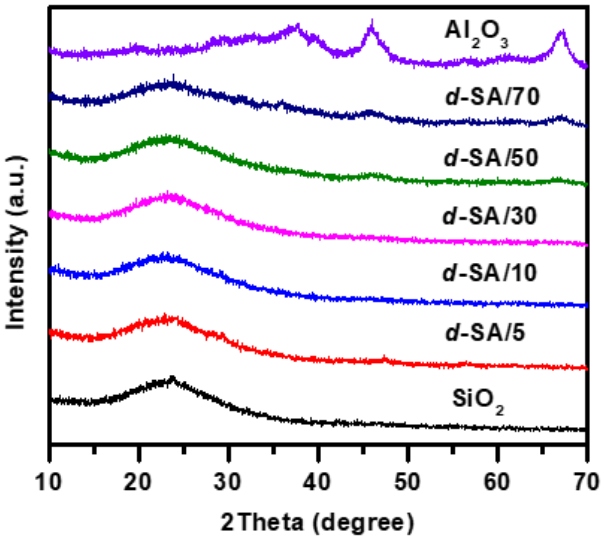

Fig. S2. XRD patterns of *d*-SA/x catalysts

HAADF images of d-SA catalysts

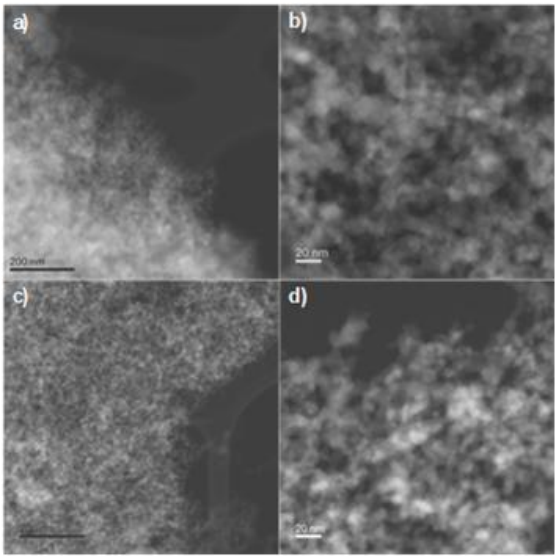

Fig. S3. HAADF images of *d*-SA/10 (a, b) and *d*-SA/50 (c,d). Scale bar: 200 nm for (a) and (c), and 20 nm for (b) and (d).

Characterization of BAS and LAS using 1H MAS NMR difference spectra

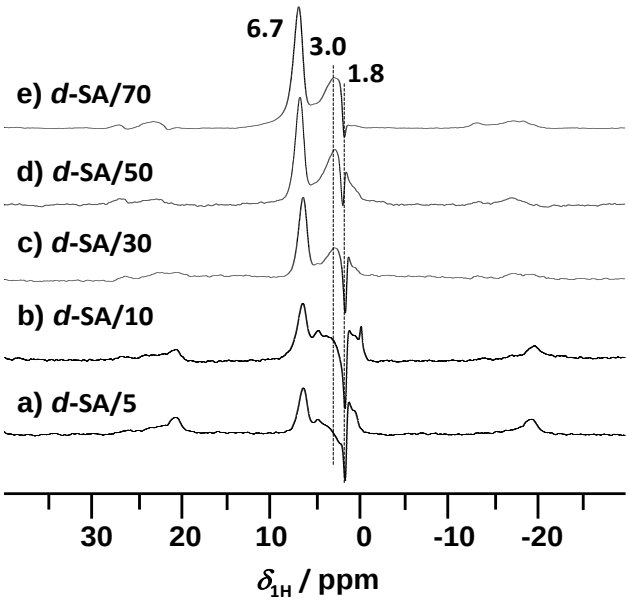

Fig. S4. ^{1}H MAS NMR difference spectra recorded before and after ammonia loading on dehydrated ASAs with different Al content.

Conversion of cyclohexanol vs. BAS density

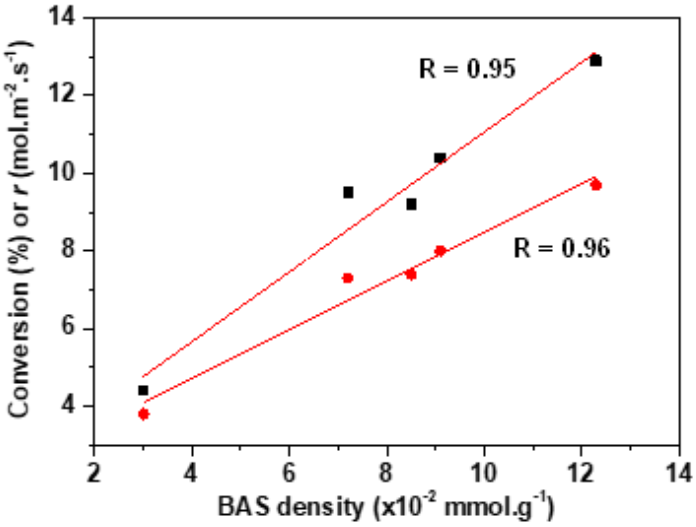

Fig. S5. Conversion of cyclohexanol (black square) and rate of cyclohexanol conversion ***r*** (red circles) versus the density of BAS on d-SA catalysts. The conversion and rate of pure alumina is subtracted from the conversion and rate of each catalyst.

Conversion of glucose vs. LAS density

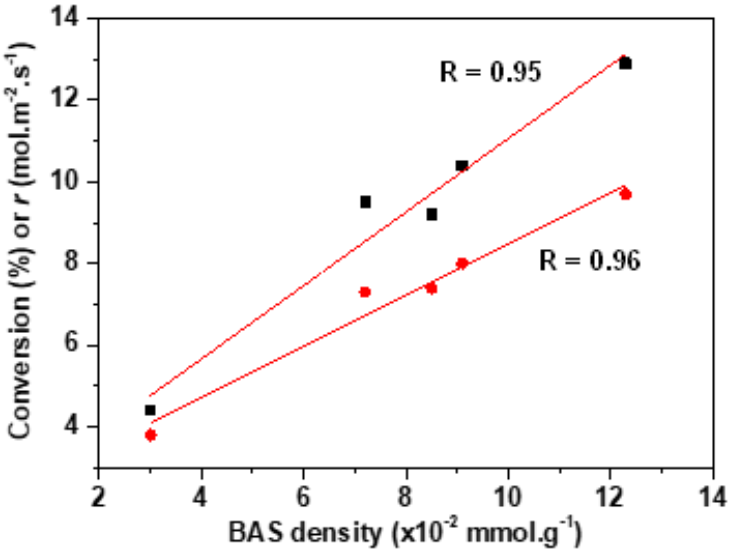

Fig. S6. The conversion of glucose vs. the density of LAS after 1.5 h of reaction.

Selectivity of HMF vs. BAS density

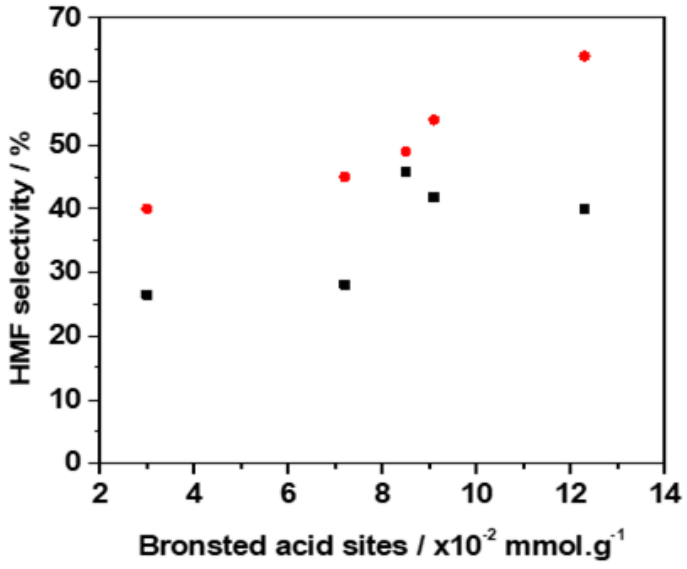

Fig. S7 The selectivity of HMF vs. the density of Brønsted acid sites after 2 h (black square) and 4 h (red circle) reaction

Recycle study over d-SA/30 catalyst

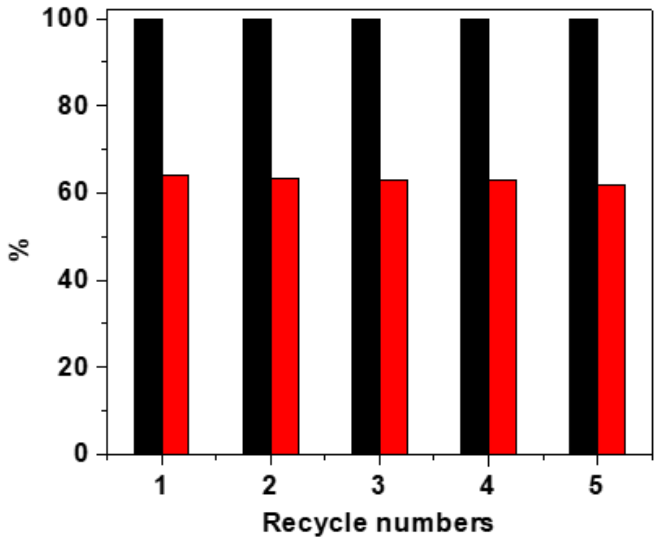

Fig. S8. *d*-SA/30: conversion of glucose (black) and selectivity of HMF (red) after 5 recycle uses.

References

[1] Huang, J.; Jiang, Y. J.; Marthala, V. R. R.; Wang, W.; Sulikowski, B.; Hunger, M. *Microporous Mesoporous Mater.* **2007**, *99*, 86-90.

[2] Wang, Z.; Wang, L.; Jiang, Y.; Hunger, M.; Huang, J. *ACS Catal.* **2014**, *4*, 1144-1147.

[3] Schimoeller, B.; Pratsinis, S.E.; Baiker, A. *ChemCatChem* 2011, 3, 1234-1256.